

Analysis of Seismoacoustic Data for the Operational Status of Two Nuclear Reactors



Chengping Chai
Omar Marcillo
Monica Maceira

April 2023



DOCUMENT AVAILABILITY

Reports produced after January 1, 1996, are generally available free via OSTI.GOV.

Website www.osti.gov

Reports produced before January 1, 1996, may be purchased by members of the public from the following source:

National Technical Information Service
5285 Port Royal Road
Springfield, VA 22161
Telephone 703-605-6000 (1-800-553-6847)
TDD 703-487-4639
Fax 703-605-6900
E-mail info@ntis.gov
Website <http://classic.ntis.gov/>

Reports are available to US Department of Energy (DOE) employees, DOE contractors, Energy Technology Data Exchange representatives, and International Nuclear Information System representatives from the following source:

Office of Scientific and Technical Information
PO Box 62
Oak Ridge, TN 37831
Telephone 865-576-8401
Fax 865-576-5728
E-mail reports@osti.gov
Website <https://www.osti.gov/>

This report was prepared as an account of work sponsored by an agency of the United States Government. Neither the United States Government nor any agency thereof, nor any of their employees, makes any warranty, express or implied, or assumes any legal liability or responsibility for the accuracy, completeness, or usefulness of any information, apparatus, product, or process disclosed, or represents that its use would not infringe privately owned rights. Reference herein to any specific commercial product, process, or service by trade name, trademark, manufacturer, or otherwise, does not necessarily constitute or imply its endorsement, recommendation, or favoring by the United States Government or any agency thereof. The views and opinions of authors expressed herein do not necessarily state or reflect those of the United States Government or any agency thereof.

Nuclear Nonproliferation Division

**ANALYSIS OF SEISMOACOUSTIC DATA FOR THE OPERATIONAL STATUS OF
TWO NUCLEAR REACTORS**

Chengping Chai
Omar Marcillo
Monica Maceira

April 2023

Prepared by
OAK RIDGE NATIONAL LABORATORY
Oak Ridge, TN 37831
managed by
UT-BATTELLE LLC
for the
US DEPARTMENT OF ENERGY
under contract DE-AC05-00OR22725

CONTENTS

LIST OF FIGURES	iv
LIST OF TABLES.....	iv
ACKNOWLEDGMENTS	v
ABSTRACT.....	1
1. INTRODUCTION	1
2. DATA	3
2.1 HFIR DATA	3
2.2 ATR DATA	3
3. SEISMOACOUSTIC ENERGY AND PHYSICAL VARIABLES.....	6
3.1 HFIR PHYSICAL VARIABLES	6
3.2 ATR PHYSICAL VARIABLES	6
4. CLUSTER ANALYSIS.....	9
4.1 HFIR CLUSTER ANALYSIS RESULTS	9
4.2 ATR CLUSTER ANALYSIS RESULTS.....	11
5. CONCLUSIONS	19
6. REFERENCES	20

LIST OF FIGURES

Figure 1. Locations of the HFIR and ATR.	2
Figure 2. Schematic showing similarities and differences between HFIR and ATR and their respective cooling towers.	2
Figure 3. The location of the seismoacoustic station, WACO.	3
Figure 4. Locations of FSAN and SSAN stations deployed for the ICE Labyrinth campaign.	4
Figure 5. ATR ICE Labyrinth data availability per station and channel.	5
Figure 6. Thermal monitoring system for HFIR that shows temperature probe sensor data for the (a) PCS, (b) SCS, (c) pool coolant system, and (d) pool cleanup system displayed over time.	7
Figure 7. Correlation between ATR Ground Truth physical variables and seismic energy for station S4.	8
Figure 8. Results of the Gaussian mixture algorithm for HFIR using the vertical seismic data from WACO.	10
Figure 9. Results of the hierarchical clustering algorithm for HFIR using the acoustic data from WACO.	11
Figure 10. The averaged spectrums of the ON and OFF group using data from station WACO based on the Gaussian mixture algorithm. (a) shows the PSDs of the seismic data. (b) shows the PSDs of the acoustic data.	12
Figure 11. Accuracies of different clustering algorithms for the vertical component of the seismic data from station WACO. A 1 h window length was used to compute spectrums.	13
Figure 12. Accuracy of different channels using the Gaussian mixture algorithm, a 1 h long window length, and data from station WACO.	13
Figure 13. Accuracy of the Gaussian mixture algorithm using the vertical component of seismic data from station WACO as a function of window length used to compute spectrum.	14
Figure 14. Results of the Gaussian mixture algorithm for ATR using the seismic data from station S4. The shaded region in panel a indicates the reactor was ON according to the ground truth data.	15
Figure 15. The averaged spectrums of the ON and OFF groups using the vertical component seismic data from station S4 based on the Gaussian mixture algorithm.	16
Figure 16. Accuracies of different clustering algorithms for the vertical component of the seismic data from station S4.	16
Figure 17. Accuracies of different channels using the Gaussian mixture algorithm, a 1 h long window length, and data from station S4.	17
Figure 18. Accuracy of the Gaussian mixture algorithm using the vertical component of seismic data from station S4 as a function of window length that was used to compute spectrum.	17
Figure 19. Accuracy of the Gaussian mixture algorithm for the vertical component seismic data from stations S1-S6 and the majority vote of all stations. A 1 h long time window was used to compute spectrum.	18

LIST OF TABLES

Table 1. Location coordinates and description for each of the Oak Ridge National Laboratory seismoacoustic stations deployed for the ICE Labyrinth campaign.	4
--	---

ACKNOWLEDGMENTS

The work described in this report was funded by the US National Nuclear Security Administration, Office of Defense Nuclear Nonproliferation Research and Development, Office of Proliferation Detection. This manuscript has been authored in part by UT-Battelle LLC, under contract DE-AC05-00OR22725 with the US Department of Energy. This research used resources at the High Flux Isotope Reactor, a US Department of Energy Office of Science User Facility operated by the Oak Ridge National Laboratory.

This research used resources of the Compute and Data Environment for Science at Oak Ridge National Laboratory, which is supported by the Office of Science of the US Department of Energy under contract DE-AC05-00OR22725.

The views and conclusions contained in this document are those of the authors and should not be interpreted as necessarily representing the official policies, either expressed or implied, of the US government. The authors acknowledge that there are no conflicts of interest recorded.

Most figures were prepared with Matplotlib version 3.4.3 (Hunter, 2007). Numpy version 1.21.2 (van der Walt et al., 2011) and ObsPy version 1.2.2 (Beyreuther et al., 2010; Krischer et al., 2015; Megies et al., 2011) were used to process the seismic and acoustic data. Figure 3 and Figure 4 used satellite images from Google Earth (<https://www.google.com/earth/>, last accessed in December 2022). GMT version 6.4 (Wessel et al., 2019) was used to create Figure 1.

The authors thank Jason Hite for reviewing this report.

ABSTRACT

Physics-based and machine-learning-based techniques have been developed to characterize power levels and material transfers using seismic and acoustic data at the High Flux Isotope Reactor. To assess the robustness and transferability of these techniques, seismoacoustic data were collected at Idaho National Laboratory's Advanced Test Reactor. Both reactors operate in cycles consisting mainly of full-power operation and end-of-cycle outage. The seismoacoustic energy was compared against physical variables from the monitoring systems at both reactors. The results demonstrate a correlation between seismic energy and reactor power level at both reactors. The authors applied k-means, hierarchical, and Gaussian mixture clustering algorithms to seismic and/or acoustic data and compared the results against ground truth information for each reactor. After several data preprocessing steps, the clustering algorithms performed reasonably well for the vertical component seismic data at both reactors. The algorithms grouped seismic and acoustic signals accurately into a group corresponding to full-power operation and another group corresponding to end-of-cycle outage. The Gaussian mixture algorithm typically outperformed the k-means and hierarchical clustering algorithms. However, k-means and hierarchical clustering algorithms produced better results in certain cases. The results demonstrate the developed techniques work at both reactors.

1. INTRODUCTION

The Multi-Informatics for Nuclear Operations Scenarios venture has a primary goal of developing and implementing multimodal data analysis approaches to improve current capabilities to assess the ability to characterize reactor power levels and nuclear material transfers. The project's test bed is the High Flux Isotope Reactor (HFIR; Figure 1) at Oak Ridge National Laboratory. For the past few years, the project's team has demonstrated that signals from multiple sensing modalities collected at the HFIR cooling tower can be used to improve estimates of operational events and the operational state of cooling tower equipment (e.g., Chai et al., 2023; Guenaga et al., 2021; Marcillo et al., 2020), and to predict HFIR power level status (e.g., Chai et al., 2022)(e.g., Chai et al. 2022) .

To assess the robustness and transferability of the data analytical methods developed under the Multi-Informatics for Nuclear Operations Scenarios project, the venture team executed the ICE Labyrinth signals collection campaign at Idaho National Laboratory's (INL's) Advanced Test Reactor (ATR; Figure 1) from January 25 to May 6, 2021. The sensors were deployed near the ATR cooling tower to take persistent measurements during the operation of a complete ATR cycle beginning in February and ending in April 2021.

ATR is a 105 MW research and isotope production nuclear reactor that operates an average of four cycles annually. HFIR is an 85 MW research and isotope production nuclear reactor that operates with cycles of 21 and 23 days. The cooling towers supporting ATR and HFIR have a similar design, but there are distinct differences in the construction and equipment used by each tower (Figure 2). The reactors have two main operation statuses—full-power operation (i.e., ON) and end-of-cycle outage (i.e., OFF). Another operation status is the intermediate status as the reactors switch from OFF to ON.

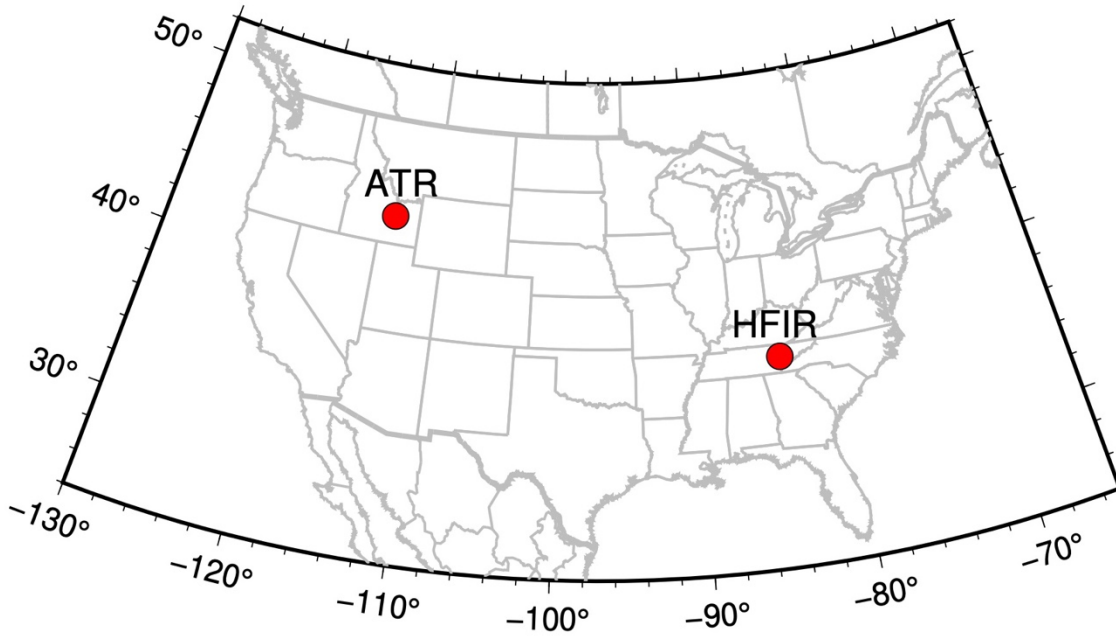


Figure 1. Locations of the HFIR and ATR.





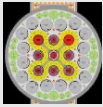

HFIR		Reactor	<ul style="list-style-type: none"> ~85 MW Start-up is typically within a few hours Annular core No electricity is produced 
		Cooling tower	<ul style="list-style-type: none"> Mechanical draft cooling tower 2 Variable speed fans 2 two speed fans 4 exposed pumps 
ATR		Reactor	<ul style="list-style-type: none"> ~105 MW Start-up is typically over a few days Serpentine core No electricity is produced 
		Cooling tower	<ul style="list-style-type: none"> Mechanical draft cooling tower 4 Variable speed fans 4 pumps inside pump room 

Figure 2. Schematic showing similarities and differences between HFIR and ATR and their respective cooling towers.

2. DATA

The team used seismoacoustic data and physical variables from the monitoring system of each reactor to investigate the correlation between seismoacoustic data and reactor power for HFIR and ATR.

2.1 HFIR DATA

The team deployed a seismoacoustic station, WACO, near the HFIR buildings (Figure 3). The station was equipped with a three-channel 4.5 Hz Geospace geophone and three Inter-Mountain Labs infrasound sensors. The station has operated since June 2017 and originally collected seismic and acoustic data with a sampling rate of 200 Hz. The sampling rate was increased to 500 Hz in November 2019. This study focused on the seismoacoustic data recorded between November 6, 2019 and February 5, 2020.



Figure 3. The location of the seismoacoustic station, WACO. The latitude and longitude of the bottom left corner of the satellite image is 35.9169° (north) and 84.3042° (west), respectively (Chai et al. 2022).

2.2 ATR DATA

Oak Ridge National Laboratory's seismoacoustic team deployed four nodal-type (FSAN) seismic stations and two seismoacoustic (SSAN) stations (S2 and S6) as part of the ATR ICE Labyrinth campaign at Idaho National Laboratory (Figure 4 and Table 1). The four FSAN stations were configured with a sampling rate of 1,000 Hz. Each of the two seismoacoustic stations comprised a three-component, low-frequency, 1 Hz Geospace GS-1 3C SeisMonitor geophone and an InfraBSU infrasound sensor. The geophone and infrasound sensors were connected to a 6-channel Nanometrics Centaur digitizer configured to sample at 1,000 Hz.



Figure 4. Locations of FSN and SSAN stations deployed for the ICE Labyrinth campaign.

Table 1. Location coordinates and description for each of the Oak Ridge National Laboratory seismoacoustic stations deployed for the ICE Labyrinth campaign.

Station	Station device	Latitude	Longitude
S1	Seismic	43.589744	-112.966571
S2	Seismoacoustic	43.589183	-112.966071
S3	Seismic	43.589756	-112.965994
S4	Seismic	43.589750	-112.967114
S5	Seismic	43.588873	-112.966427
S6	Seismoacoustic	43.588980	-112.967060

3. SEISMOACOUSTIC ENERGY AND PHYSICAL VARIABLES

3.1 HFIR PHYSICAL VARIABLES

Analyses of the data collected at HFIR (together with ground truth information) helped answer the questions related to HFIR's power level status and the association of seismoacoustic signals with the operation of specific ancillary equipment related to the functioning of the reactor. Marcillo et al. (2020) found that the overall seismoacoustic energy closely follows the main power cycle of the reactor and identified spectral regions excited by specific reactor operational conditions. In particular, the authors identified a tonal noise sequence with a fundamental frequency around 21.4 Hz and multiple harmonics that emerge as the reactor reaches 90% of nominal power in both seismic and acoustic channels. The team also used temperature measurements from the monitoring system of the reactor to suggest links between the operation of reactor's subsystems and seismoacoustic signals. Figure 5 shows the temperature measurements from the reactor monitoring system grouped by subsystems. All thermal channels are plotted using the same color scale for reference. The black ticks at the top of each panel show the time of startup and shutdown. In general, the figure shows a clear pattern of higher temperatures (for the majority

of signals) during full-power operations at the primary cooling system (PCS) and secondary cooling system (SCS), whereas the pool coolant system signals are almost constant.

3.2 ATR PHYSICAL VARIABLES

Following the approach used by Marcillo et al. (2020), the team used signals from the monitoring system and seismic signals at ATR to estimate the level of correlation between physical variables (e.g., temperature of the coolant, fan speeds) and seismic energy (similar to Figure 5). The estimation uses the Pearson correlation coefficient between the monitoring system and the seismic or acoustic root mean square. Figure 6(a) shows the different variables of the monitoring system sorted by the correlation coefficient (with the highest and lowest correlation coefficients at the bottom and top of the plot, respectively). Figure 6(b) shows the time evolution of the variables of the monitoring system normalized by each variable to show changes in the physical units relative to one another. Two very distinct groups were recorded—signals that are inversely proportional to root mean square (top of the panel), and signals with a high positive correlation coefficient (bottom of the panel).

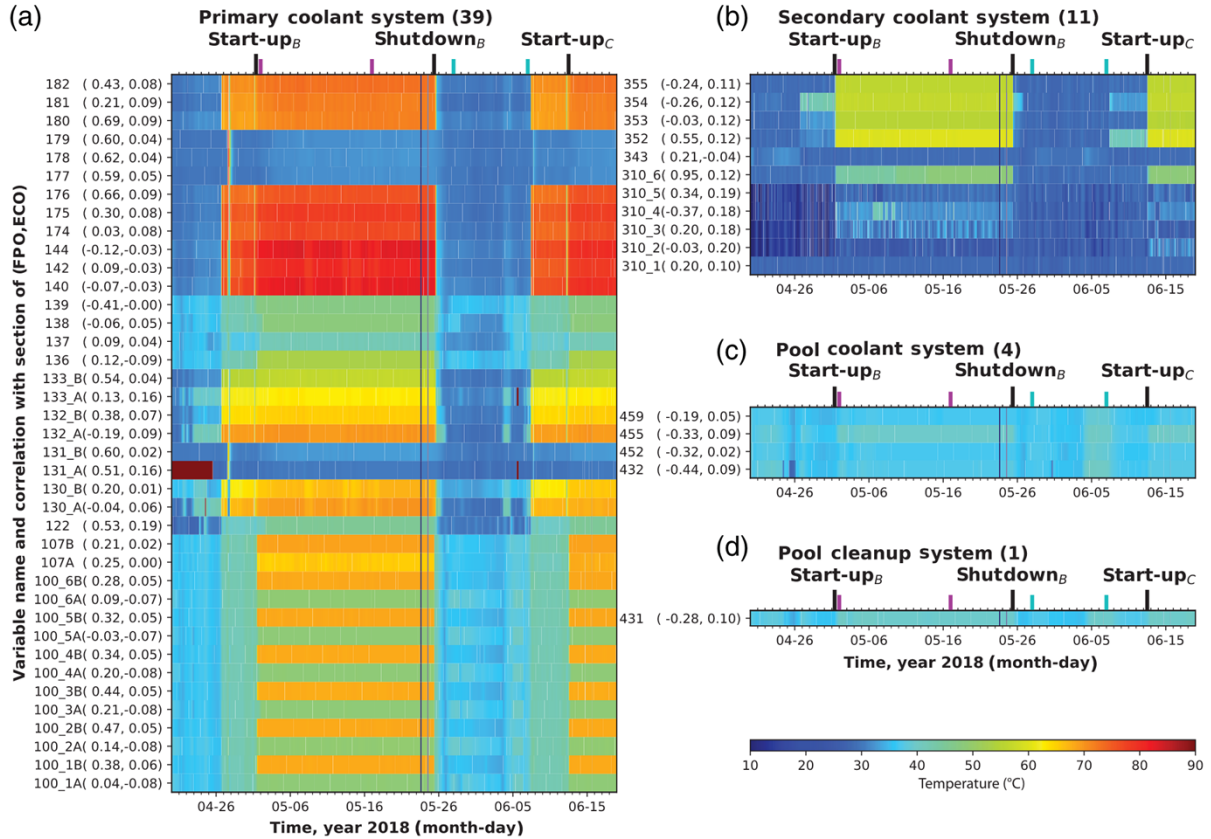


Figure 5. Thermal monitoring system for HFIR that shows temperature probe sensor data for the (a) PCS, (b) SCS, (c) pool coolant system, and (d) pool cleanup system displayed over time. Correlation values between thermal signals and root mean square seismic signals are displayed in parentheses next to the variable name for correlations with regions within full-power operation (between magenta lines) and end-of-cycle outage (between cyan lines) (Marcillo et al., 2020).

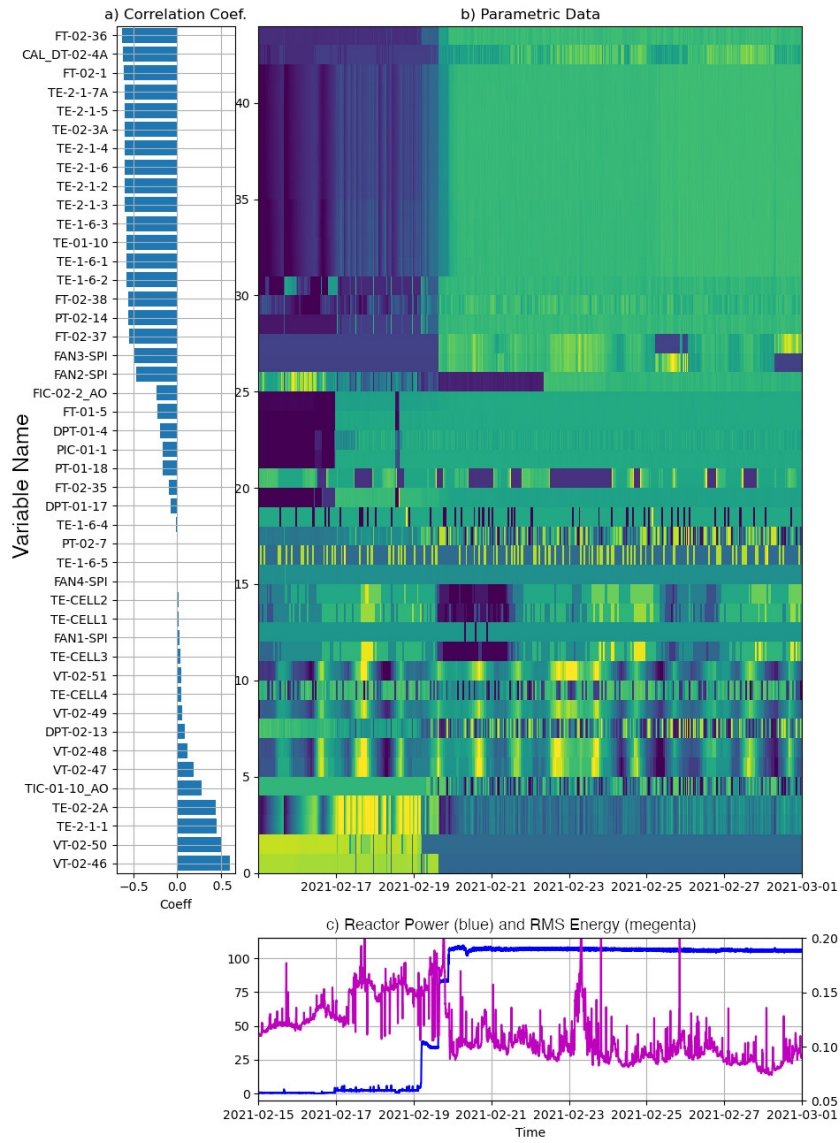


Figure 6. Correlation between ATR Ground Truth physical variables and seismic energy for station S4.

4. CLUSTER ANALYSIS

The team applied three clustering algorithms to seismic data collected at HFIR and ATR to infer the main status of the reactor (ON or OFF). The tested algorithms include k-means, hierarchical, and Gaussian mixture clustering. The team first converted the continuous seismograms into spectrums with a window length of 10 s using a fast Fourier transform algorithm. The resulting spectrums were then averaged within a longer window length to reduce the background noise variations. Since a few thousand data points were in each spectrum, the team performed principal component analysis to reduce the dimension of the spectrums while preserving most of the information. Thus, the spectrums were converted into corresponding principal components. We selected the number of principal components that comprise 80% of the total variance of the spectrums. The exact number of principal components changed with the input dataset. Approximately 10 principal components were used by the clustering algorithms. The number of clusters was fixed at two since the team focused on the two main operational statuses of the reactors.

4.1 HFIR CLUSTER ANALYSIS RESULTS

For HFIR, the team used the seismic and acoustic data recorded at WACO. Using seismic data alone, all three algorithms clustered the seismic signals correctly into a group related to reactor ON and another group related to reactor OFF. As shown in Figure 7, the seismic spectrogram of the vertical component from WACO shows different patterns when the reactor is ON compared to when the reactor is OFF. However, the pattern changes irregularly with time. As clustering is usually used for data exploration, accuracies for clustering algorithms are typically not available. Since we have ground truth information (operational logs), we compare cluster assignments against ground truth labels to quantify the performance of clustering algorithms. The Gaussian mixture algorithm can separate the ON and OFF groups with very high accuracies (larger than 0.99) when we used a 1 h window length for the spectrum averaging. The acoustic spectrogram exhibits different patterns than the seismic spectrogram (Figure 8). These patterns are not as clear as those on the seismic spectrogram. The hierarchical clustering algorithm produced perfect accuracy for the ON group but did not perform well (with an accuracy of 0.847) for the OFF group when applied to the acoustic data. The poor performance of hierarchical clustering for the OFF group may be due to long-lasting high-power patterns in the spectrogram for late December 2019. The team also computed the average of all the spectrums for the ON group and the OFF group. Higher power was observed when the reactor was ON and relatively lower power when the reactor was OFF for both seismic and acoustic data in a broad frequency band (Figure 9).

Because the choice of clustering algorithm, the data channel, and the averaging window length affect the performance of the algorithm, the team compared the accuracies of clustering results with different algorithms, data channels, and window lengths. All three clustering algorithms performed well for the vertical component seismic data from WACO. The Gaussian mixture algorithm had a slightly higher accuracy than the other two algorithms (Figure 10). The vertical component seismic data provided better clustering results than the horizontal seismic components and the acoustic data (Figure 11) when the other parameters were kept the same. The Gaussian mixture algorithm performed well with window lengths of 1 h, 30 min, and 15 min (Figure 12). The accuracy of the OFF group was poor with a window length of 5 min, which may be because of large amplitude variations in background noise when shorter window lengths were used. The ratio of data samples between the ON group and the OFF group may also affect the performance.

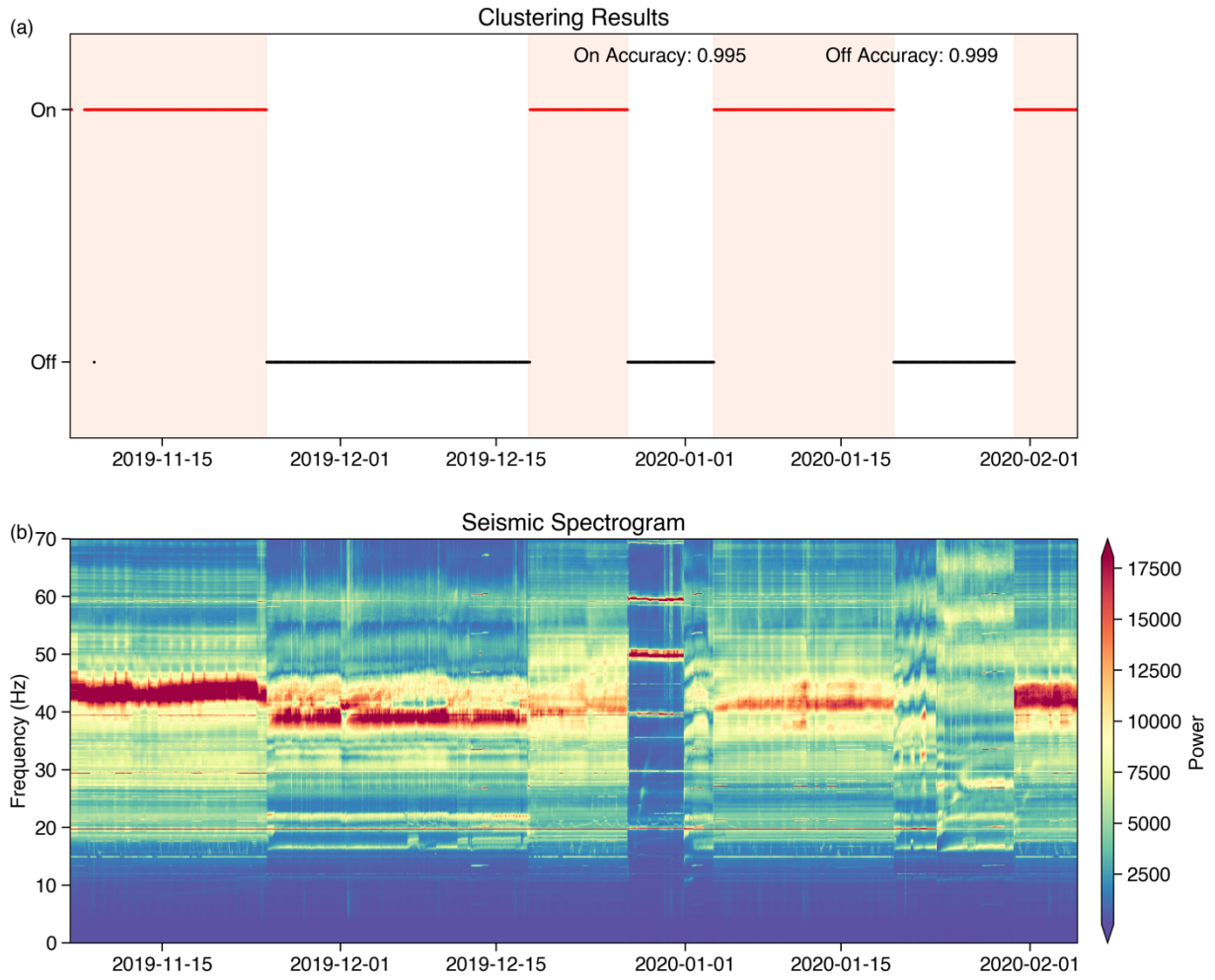


Figure 7. Results of the Gaussian mixture algorithm for HFIR using the vertical seismic data from WACO.
The shaded region in (a) indicates the reactor was ON according to the ground truth data.

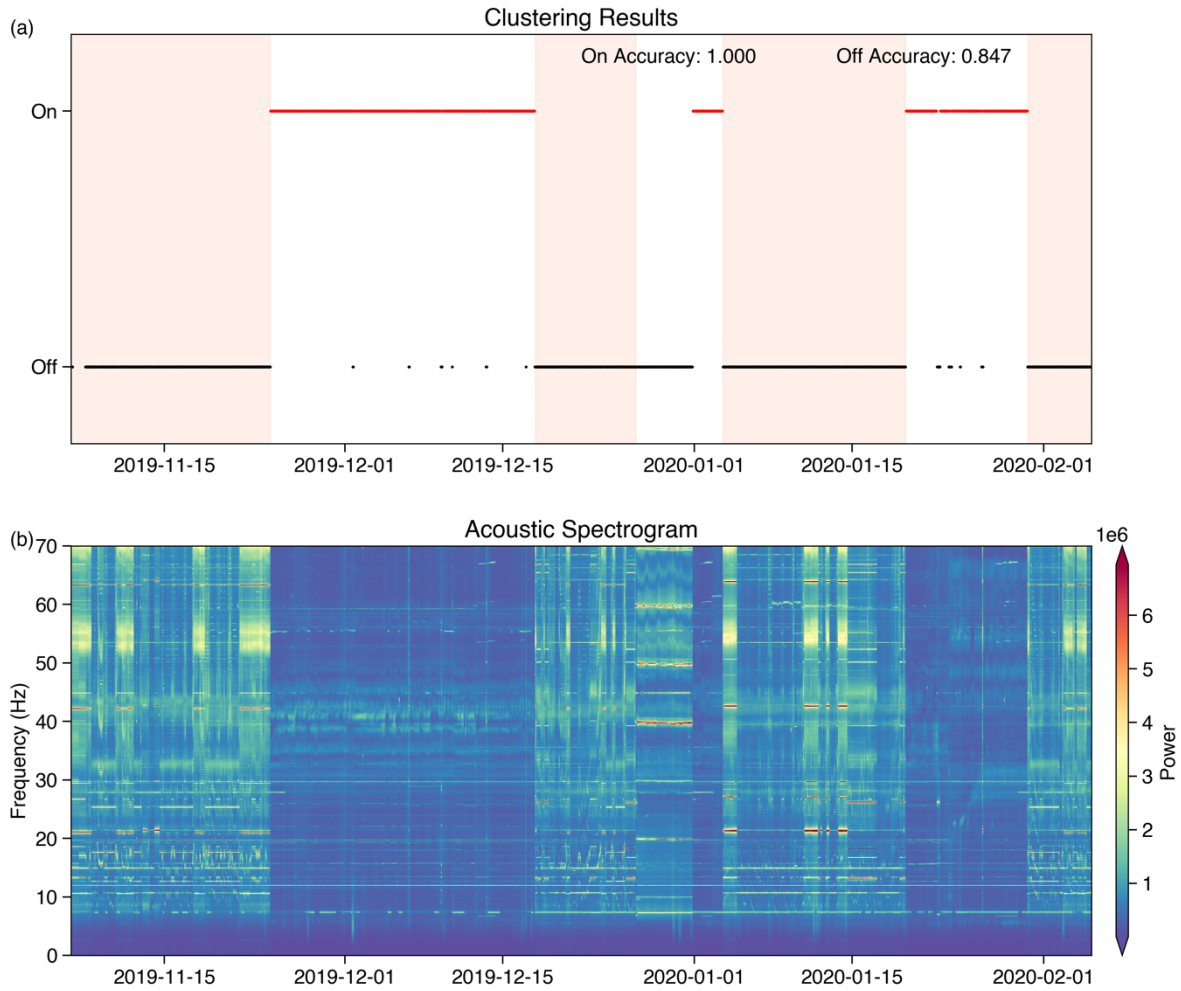


Figure 8. Results of the hierarchical clustering algorithm for HFIR using the acoustic data from WACO.
The shaded region in (a) indicates the reactor was ON according to the ground truth data.

4.2 ATR CLUSTER ANALYSIS RESULTS

The team applied the same algorithms with identical parameters to seismic data collected from the seismic stations at ATR. Unfortunately, the acoustic data from station S2 did not have coverage for the entire cycle. The acoustic data from station S6 were dominated by high energy local noise. We focus only on seismic data for ATR stations. As shown in Figure 13, the seismic spectrograms for station S4 had different patterns compared with those for WACO. At WACO, the seismic energy was higher when the reactor was ON. At station S4, the recorded seismic energy was lower between 5 and 50 Hz when the reactor was ON. Despite this significant difference in seismic data and difference in sampling rate, the Gaussian mixture algorithm performed reasonably well with an accuracy within 0.967 for the ON group and 0.987 for the OFF group (Figure 13). The averaged spectrums of the ON and OFF groups indicate that the recorded seismic energy for the ON group was lower for frequencies below 100 Hz (Figure 14). However, the seismic energy of the ON group was higher than the OFF group for frequencies of 120–180 Hz and 240–420 Hz.

A comparison of the three clustering algorithms using the vertical component of the seismic data from station S4 suggests that all three algorithms produced satisfactory results (Figure 15). The Gaussian mixture algorithm reached an accuracy within 0.967 for the ON group and 0.987 for the OFF group. Like the results for WACO, the vertical component seismic channel of station S4 had much better clustering results than the horizontal channels (Figure 16). Unlike the results for WACO, the Gaussian mixture algorithm performed well for all the averaging window lengths tested on the data from station S4 (Figure 17). One possible reason for the better clustering results for station S4 is the station's higher sampling rate. With a higher sampling rate, a finer resolution is possible in the frequency domain, which may improve the clustering results. Among the six stations at ATR, stations S2, S3, S4, and S5 performed well with the Gaussian mixture algorithm (Figure 18). The k-means and hierarchical clustering algorithms led to accuracies within higher than 0.9 for both ON and OFF groups for the seismic data from station S1. The poor performance of the Gaussian mixture algorithm at station S1 may be due to the data gaps. Significant local noise occurred in the seismic spectrogram of station S6, which could be why all the clustering algorithms did not work well there. We can use the majority vote of all the stations to obtain more stable results. As shown in Figure 18, we achieved a accuracy of 0.948 for the ON group and 0.991 for the OFF group using all the stations.

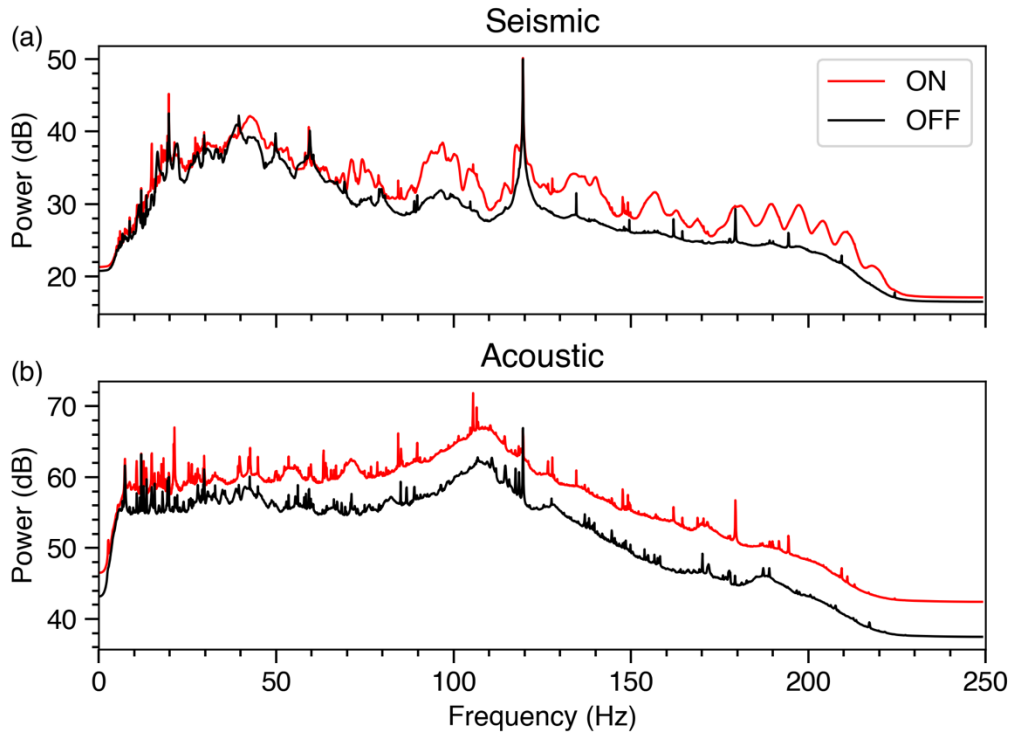


Figure 9. The averaged spectrums of the ON and OFF group using data from station WACO based on the Gaussian mixture algorithm. (a) shows the PSDs of the seismic data. (b) shows the PSDs of the acoustic data.

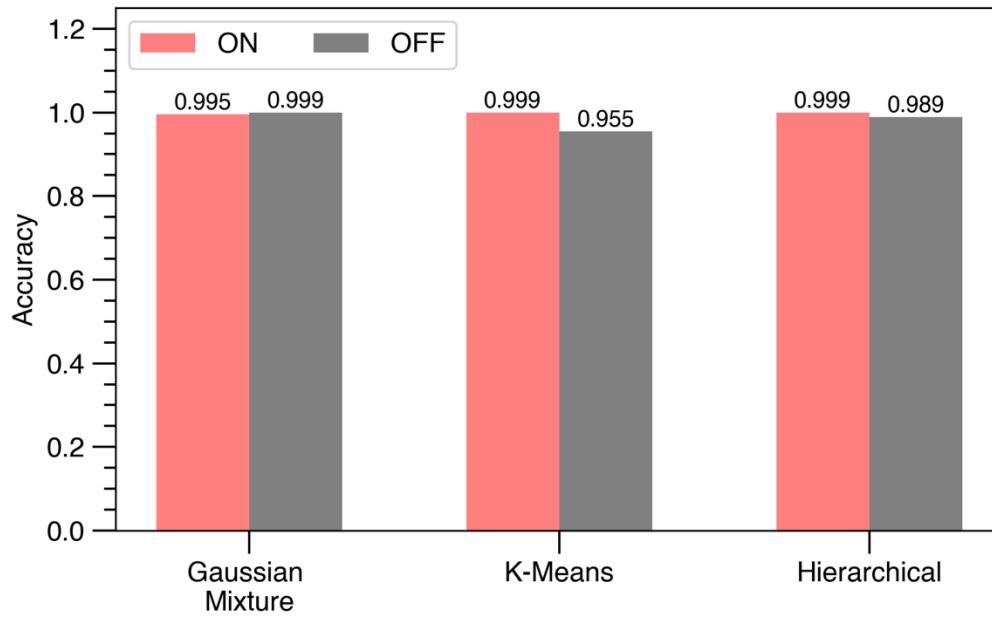


Figure 10. Accuracies of different clustering algorithms for the vertical component of the seismic data from station WACO. A 1 h window length was used to compute spectrums.

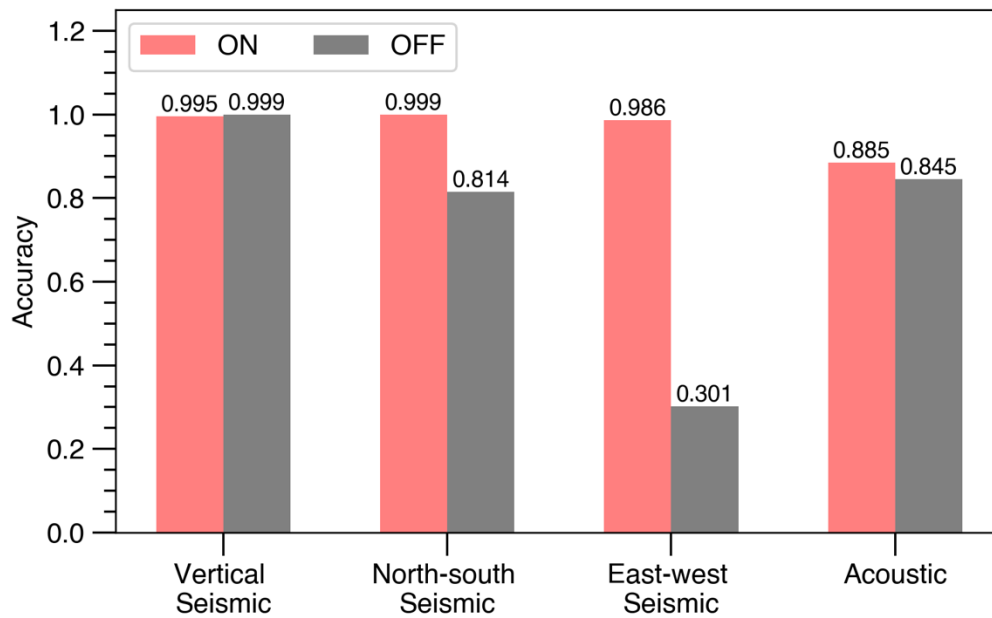


Figure 11. Accuracy of different channels using the Gaussian mixture algorithm, a 1 h long window length, and data from station WACO.

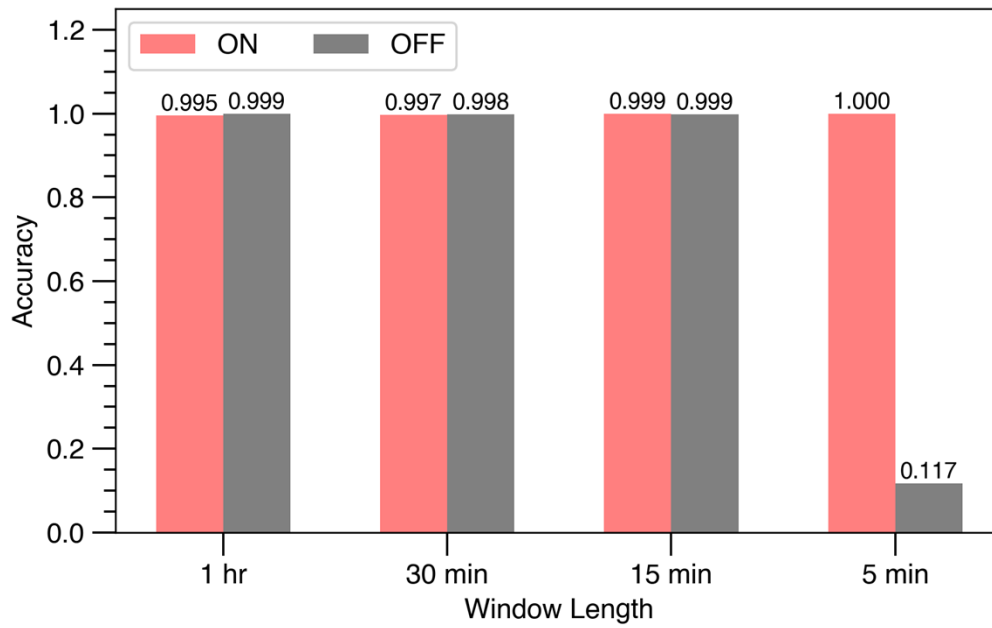


Figure 12. Accuracy of the Gaussian mixture algorithm using the vertical component of seismic data from station WACO as a function of window length used to compute spectrum.

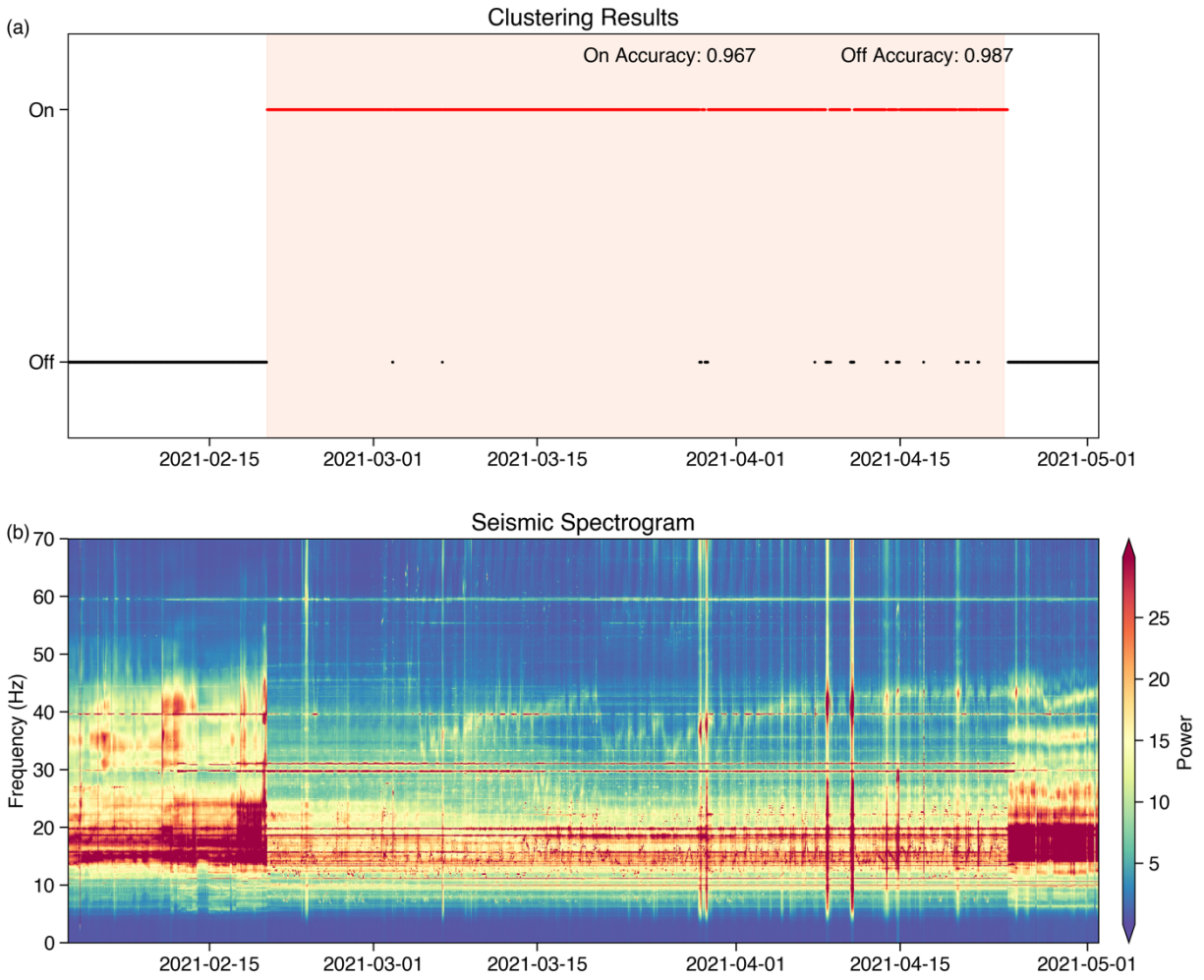


Figure 13. Results of the Gaussian mixture algorithm for ATR using the seismic data from station S4. The shaded region in panel a indicates the reactor was ON according to the ground truth data.

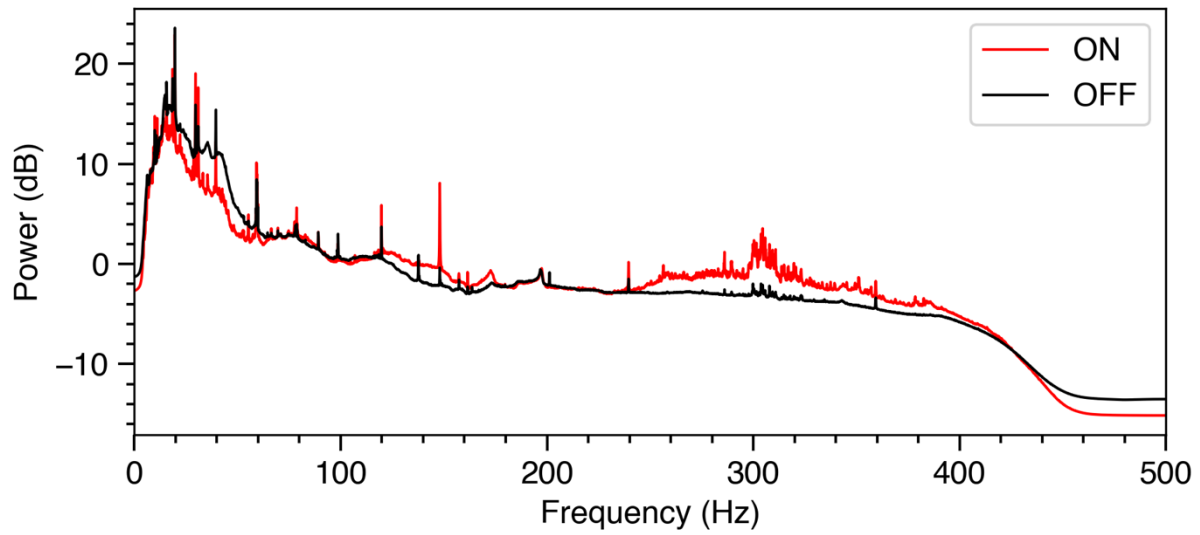


Figure 14. The averaged spectrums of the ON and OFF groups using the vertical component seismic data from station S4 based on the Gaussian mixture algorithm.

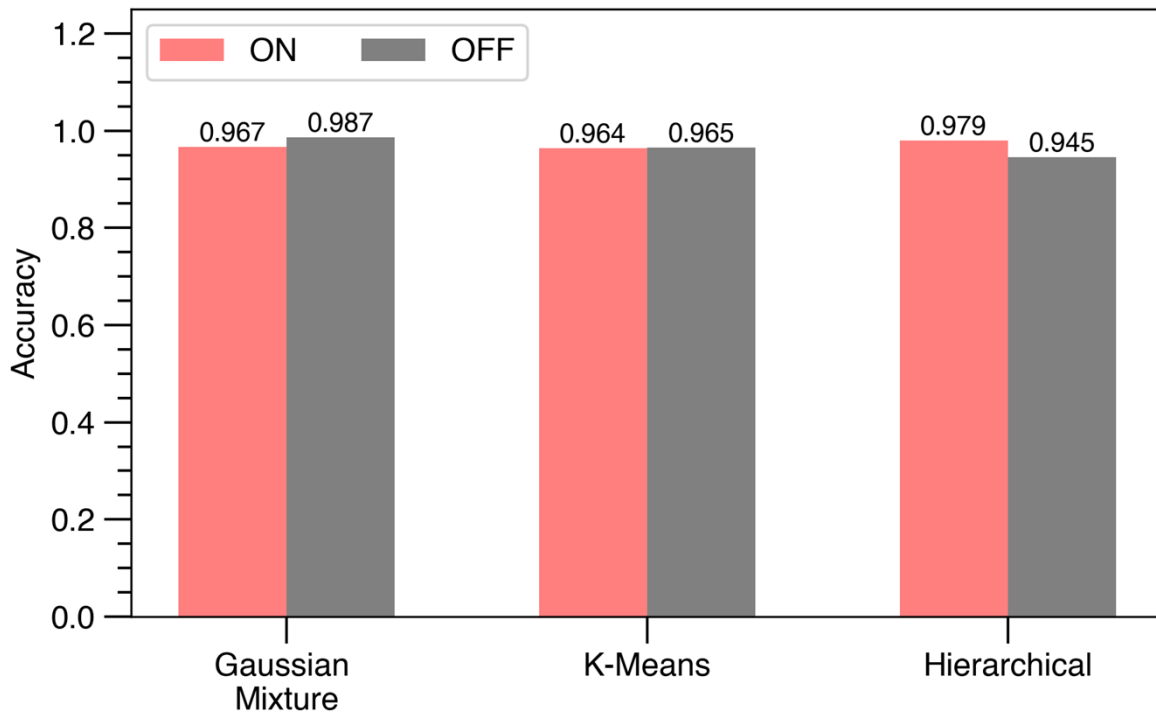


Figure 15. Accuracies of different clustering algorithms for the vertical component of the seismic data from station S4. A 1 h window length was used to compute spectrums.

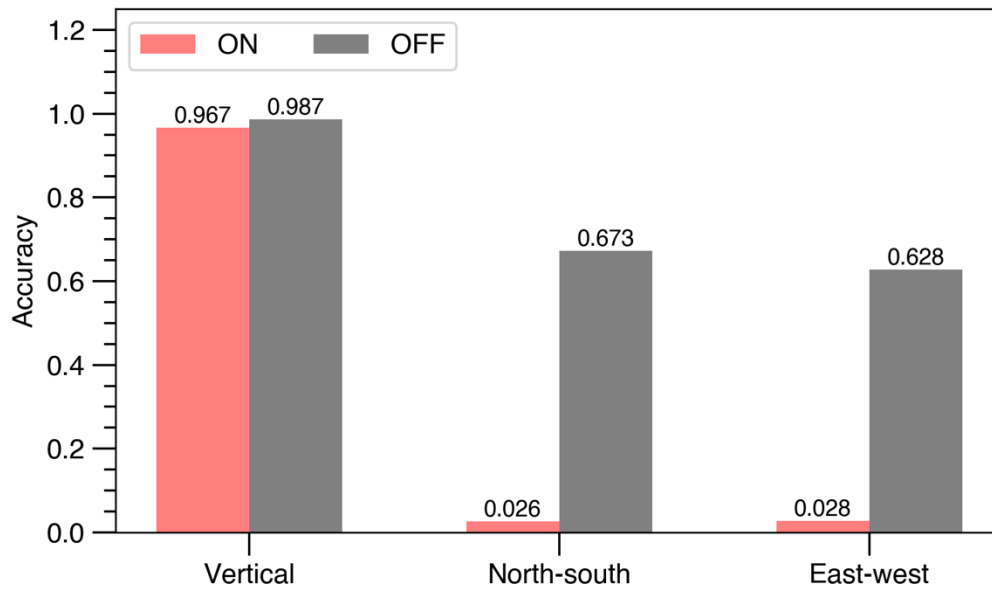


Figure 16. Accuracies of different channels using the Gaussian mixture algorithm, a 1 h long window length, and data from station S4.

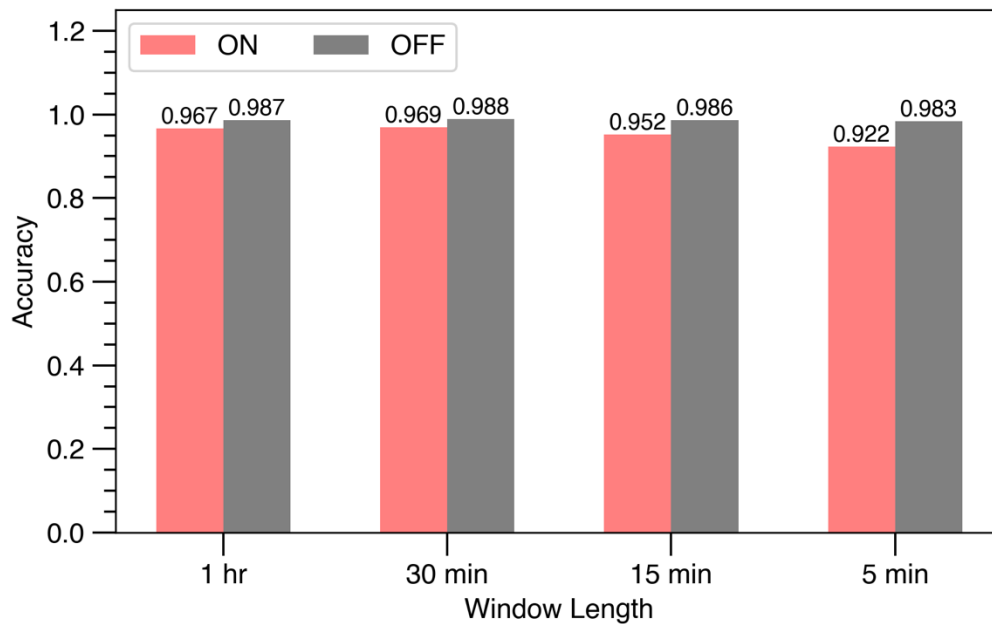


Figure 17. Accuracy of the Gaussian mixture algorithm using the vertical component of seismic data from station S4 as a function of window length that was used to compute spectrum.

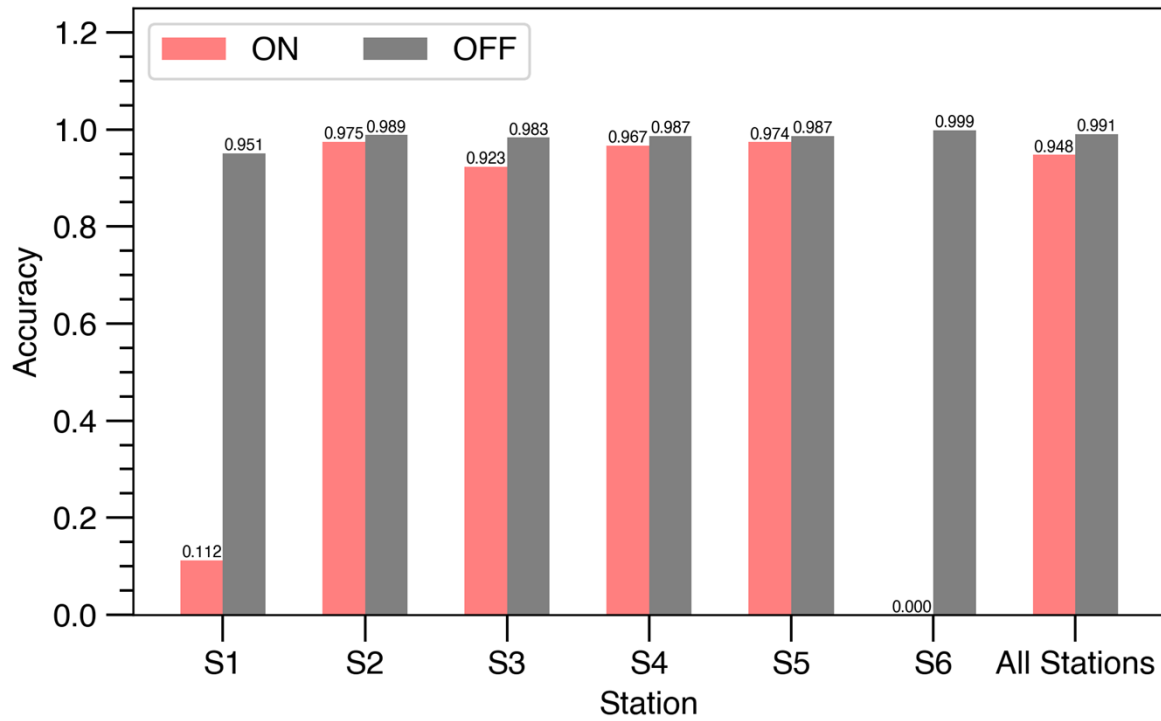


Figure 18. Accuracy of the Gaussian mixture algorithm for the vertical component seismic data from stations S1-S6 and the majority vote of all stations. A 1 h long time window was used to compute spectrum.

5. CONCLUSIONS

To assess the transferability of seismoacoustic techniques developed for HFIR, the team applied the same physic-based and machine learning-based algorithms to data from ATR. The results demonstrate that the seismic energy correlates with reactor power at both reactors. The team preprocessed the seismic and acoustic data and used principal component analysis to reduce the input data dimensions. The resulting data features were used by clustering algorithms to group seismic and acoustic data into a full-power operation group (ON) and an end-of-cycle outage group (OFF). Despite significant differences in the recorded data, the clustering algorithms performed well in most cases for both reactors. The Gaussian mixture algorithm led to slightly better clustering results than the k-means and hierarchical clustering algorithms. The vertical component of the seismic data produced much better clustering results than the horizontal components and the acoustic data. In certain cases, k-means and hierarchical clustering algorithms performed better than the Gaussian mixture algorithm. The clustering algorithms may not work as expected if large-amplitude seismic noise is recorded at a station. We applied the clustering algorithms to data that contain at least one complete cycle (with both the ON and OFF groups). If new data are collected, the algorithms should be applied to all the available data including historical data. An alternate approach is to assign labels for the new data based on the distances to the two cluster centroids that we processed.

6. REFERENCES

- Beyreuther, M., Barsch, R., Krischer, L., Megies, T., Behr, Y., & Wassermann, J. (2010). ObsPy: A Python Toolbox for Seismology. *Seismological Research Letters*, 81(3), 530–533. <https://doi.org/10.1785/gssrl.81.3.530>
- Chai, C., Ramirez, C., Maceira, M., & Marcillo, O. (2022). Monitoring Operational States of a Nuclear Reactor Using Seismoacoustic Signatures and Machine Learning. *Seismological Research Letters*, 93(3), 1660–1672. <https://doi.org/10.1785/0220210294>
- Chai, C., Marcillo, O., Maceira, M., Young, C., & Karnowski, T. (2023). Locating Operational Events of the Cooling Tower of a Nuclear Reactor with a Very Local Seismic Network. *Bulletin of the Seismological Society of America*. <https://doi.org/10.1785/0120220216>
- Guenaga, D. L., Chai, C., Maceira, M., Marcillo, O. E., & Velasco, A. A. (2021). Seismically Detecting Nuclear Reactor Operations Using a Power Spectral Density (PSD) Misfit Detector. *Bulletin of the Seismological Society of America*, 111(3), 1378–1391. <https://doi.org/10.1785/0120200267>
- Hunter, J. D. (2007). Matplotlib: A 2D Graphics Environment. *Computing in Science & Engineering*, 9(03), 90–95. <https://doi.org/10.1109/MCSE.2007.55>
- Krischer, L., Megies, T., Barsch, R., Beyreuther, M., Lecocq, T., Caudron, C., & Wassermann, J. (2015). ObsPy: a bridge for seismology into the scientific Python ecosystem. *Computational Science & Discovery*, 8(1), 014003. <https://doi.org/10.1088/1749-4699/8/1/014003>
- Marcillo, O. E., Maceira, M., Chai, C., Gammans, C., Hunley, R., & Young, C. (2020). The Local Seismoacoustic Wavefield of a Research Nuclear Reactor and Its Response to Reactor Power Level. *Seismological Research Letters*, 92(1), 378–387. <https://doi.org/10.1785/0220200139>
- Megies, T., Beyreuther, M., Barsch, R., Krischer, L., & Wassermann, J. (2011). ObsPy – What can it do for data centers and observatories? *Annals of Geophysics*, 54(1), 47–58. <https://doi.org/10.4401/ag-4838>
- van der Walt, S., Colbert, S. C., & Varoquaux, G. (2011). The NumPy Array: A Structure for Efficient Numerical Computation. *Computing in Science & Engineering*, 13(2), 22–30. <https://doi.org/10.1109/MCSE.2011.37>
- Wessel, P., Luis, J. F., Uieda, L., Scharroo, R., Wobbe, F., Smith, W. H. F., & Tian, D. (2019). The Generic Mapping Tools Version 6. *Geochemistry, Geophysics, Geosystems*, 20(11), 5556–5564. <https://doi.org/10.1029/2019GC008515>

